Carpathian Journal of Earth and Environmental Sciences, February 2020, Vol. 15, No. 1, p. 261 - 273; Doi:10.26471/cjees/2020/015/127

DELINEATING THE STRUCTURAL FRAMEWORK OF THE NORTHEASTERN SINAI USING GRAVITY AND MAGNETIC DATA

Saada Ahmed SAADA[1], Ahmed A. AZAB[2], Ibrahim Nasr EL-SAYED[1] & Sherif KHARBISH[1]

[1]Faculty of Science, Geology Department, Suez University, Suez, Egypt. E-mail: Saada.elsayed@suezuniv.edu.eg
[2]Egyptian Petroleum Research Institute.

Abstract: The northern part of Sinai is studied to detect the structural elements controlling it and evaluate the distribution and the thickness of the sedimentary cover, which has an important role in both crude oil and water explorations. Therefore, gravity and magnetic data of the area were analyzed by different techniques. Besides, a structure tectonic map was established depending on the integration of the available data. The trend analysis technique was applied to gravity and magnetic data to detect major tectonic and structural trends. Fast Fourier Transform is used to calculate the regional and residual components. Moreover, the depth estimation of the basement rocks was carried out by applying a spectral analysis technique along 57 gravity and magnetic profiles. The deduced fault trends indicate the obvious effect of the Syrian Arc and the East-African tectonic trends on the area. The constructed structure map shows alternated uplifted and down faulted striped blocks, trending mainly in the NNE-SSW direction. The depth to the basement rocks ranges between 2 and 8 km. The 2D gravity and magnetic modeling indicates low magnetic susceptibility indicating granitic basement rocks. The area contains promising sites for hydrocarbon accumulation due to its thick sedimentary cover, in addition to alternated uplifted and down faulted blocks.

Key words: Sinai Peninsula; potential fields; geologic structure; data analysis; Fast Fourier Transform.

1. INTRODUCTION

The area of study is located in the Sinai Peninsula in the northeastern most part (Fig. 1). This study aims to investigate the nature and the structure of the uppermost part of the crust as well as the sedimentary cover, besides, to construct a basement structure map and structure modeling through two profiles.

Due to its importance, northern Sinai attracted the interest of many researchers (Shata, 1956; Said, 1990; Al Far, 1966; Neev, 1975, 1977 (Neev 1977); Beyth, 1981; Jenkins et al., 1982; Ammar & Afifi, 1992; Zaghloul & Khidr, 1992; Selim, 2015; Rabeh & Khalil, 2015).

Oil exploration in Sinai started at 1910 with a dry hole Tanka-1 near an oil seep in west Sinai drilled by the Sinai Petroleum Syndicate (EGPC, 1986). Since then, the Anglo Egyptian Oil Fields, Standard Oil of Egypt and the Socony Vacuum Oil Company (the Egyptian subsidiaries of Shell, Esso, and Mobil, respectively) made a detailed surface geologic mapping by gravity and magnetic surveys and drilled several wells in the central and northern Sinai without any success. Additional gravity, magnetic and seismic surveys over the north Sinai during the occupation of Sinai by Israel (1967-1979), resulted in the discovery of the Sadot gas field in 1975. Tineh, Port Fouad, Abu Zakin, Wakar, South Rafah and Mango oil and gas discoveries declared as results of exploration rights that were given by the Egyptian General Petroleum Corporation (EGPC) since 1979. Moreover, several wells have encountered promising oil and/or gas indications (EGPC, 1986).

The available data used in this study include the gravity and aeromagnetic maps, aided by the surface and subsurface geophysical and geological information implied on the surrounding area investigation. These data are analyzed and interpreted qualitatively and quantitatively through the following stages, (a) qualitative description of the gravity and magnetic maps; (b) trend analysis; (c) isolation of gravity and magnetic anomalies into their regional

and residual components using the fast Fourier transform (FFT), which is an efficient algorithm used to compute the discrete Fourier transform and the inverse discrete Fourier transform; (d) depth estimation to the causative bodies using 57 gravity and magnetic profiles that cover the area, using spectral analysis technique; (e) construction of basement structure map; (f) deducing 2-D magnetic-gravity modeling along two profiles extended across the area.

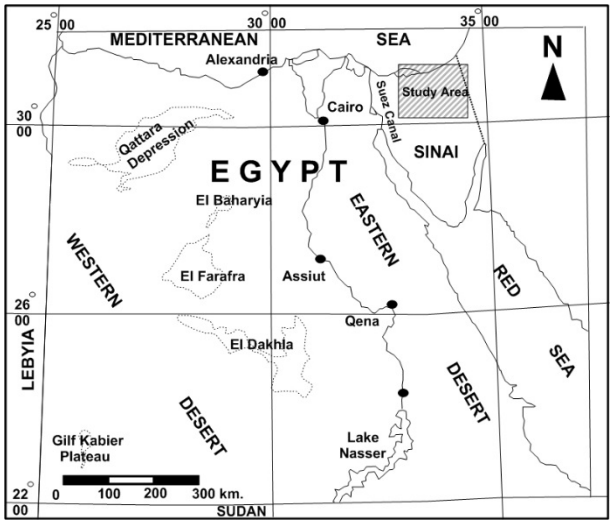

Figure 1. Location map of the study area.

2. GEOLOGICAL SETTING

Sinai is an Egyptian province located in the most northeastern part of Egypt. It occupies about 61,000 Km^2, with a triangular shape, its apex in the south at the junction between Suez and Aqaba gulfs. The triangle base is located in the north of the Mediterranean Sea. It is surrounded by the Gulf of Suez, the Suez Canal to the west and the Gulf of Aqaba, Israel, and Gaza Strip to the east. The area under investigation lies between longitudes 33^o 00', 34^{o}20'N and latitudes 30^{o}30', 31^{o}15' at the northeastern most part of Sinai (Fig. 1). It is covered by outcropped sediments from different geological times, extended from Recent time back to Jurassic (Fig. 2). The stratigraphic column of the area includes a representation of the geological time sediment from Triassic to Recent (Fig. 3). Aerial photos reveal many geological features represented by a lot of geomorphologic and super facial structures. The Sinai Peninsula is divided into three districts; the southern Sinai is one of the major Precambrian basement outcrops in Egypt with high dissected mountains of igneous and metamorphic uplifted blocks (Said, 1962; El-Shazly et al., 1974; Smith, 1984). These blocks have elevations of 2637 m (Saint Katherine); 2438m (El-Thabt) and 2285m (Mousa Mountain).

The central part of Sinai is covered by Mesozoic-Tertiary sediments with a general slope towards the north (Said, 1962; Smith, 1984). Northern Sinai has a stratigraphic section ranges from Precambrian to Recent with a thickness of 2000 m at south mainly continental facies and about 8000 m of marine facies at the north (Sharhan & Salah, 1996).

Tectonically, Sinai Peninsula is bounded by major tectonic elements that affected to a great extent its structures. These elements have been subdivided chronologically into four tectonic phases as follows:

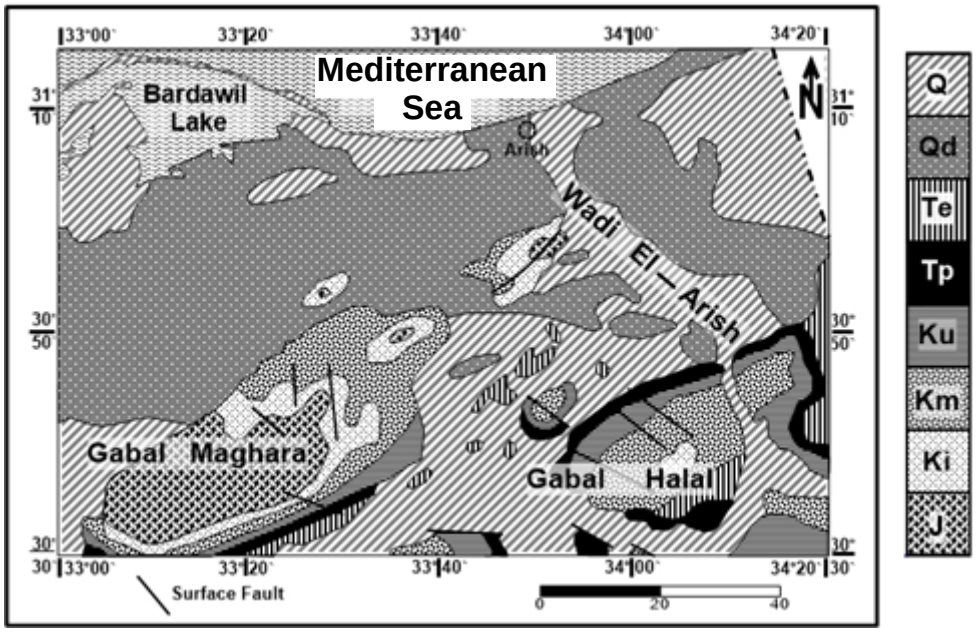

Figure 2. Geologic map of the study area: Q. Undivided Quaternary deposits, Qd. Sand Dunes, Te. Eocene, Tp. Palaeocene Ku. Upper Cretaceous, Km Middle Cretaceous, Kl. Lower Cretaceous, J. Jurassic (EGS, 1981).

(A) *Pelusium megashear (Precambrian* time). It is a system of an echelon left-lateral mega shear from Precambrian times. It extends from north at Turkey to South Atlantic Ocean crossing sub-parallel to the eastern margin of the Mediterranean Sea then reorienting northeast - southeast from Nile Delta to the Niger Delta in the Gulf of Guinea (Neev et al., 1982).

(B) *Opening of the Tethys*, in Triassic-Liassic time the rifting of north Africa-Arabia and Tethys opening occurred and caused rejuvenation of ENE-WSW deep-seated faults, consequently, the Mediterranean Basin originated from this rifting at Early Mesozoic time (Monod et al., 1974; Hsu 1977; Bein & Gvirtzmann, 1977; Biju-Duval et al., 1977; Biju-Duval & Dercourt, 1980).

(C) *Syrian Arc system*, these tectonics formed by a sequenced close, parallel asymmetrical NE to ENE oriented double plunged anticlines, trending N65° to 85° E that resulted in the main highs of the area, as a result of west-northwest movement of Africa relative to Eurasia during Laramide time (the Late Cretaceous to Early Tertiary), which closed the Tethys Sea and made a right-lateral shear displacement between North Africa and Eurasia (Smith, 1971).

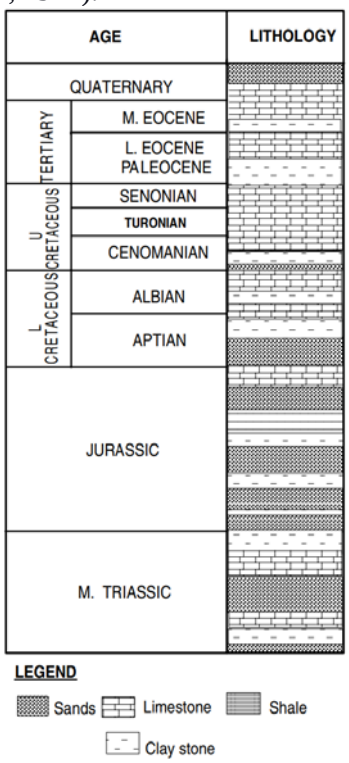

Figure 3. Generalized stratigraphic column for the northern Sinai area after (Barakat, 1982).

(D) *Gulf of Suez, there* is a general agreement that states, the major rifting associated with the Gulf of Suez initiated in the late Oligocene to early Miocene Time (e.g. Robson, 1971; Chenet & Letouzey, 1983; Steckler, 1985). It is believed that the rift created by the anticlockwise rotation movement of the Arabian plate diverging from Africa, the axis of this rotation movement located at the central or south-central Mediterranean Sea (McKenzie et al., 1970; Freund et al., 1970; Le Pichon & Francheteau, 1978).

(E) *Gulf of Aqaba*, at the southeastern edge of Sinai we find the Gulf of Aqaba. Gulf of Aqaba has a very obvious effect on the tectonic trends in the Sinai Peninsula. Aqaba Gulf was formed at a later time after the Gulf of Suez rifting; it was formed at Pliocene time (Morgan, 1990). Aqaba Gulf lied on the Dead Sea Transform Fault System; this system is a north-south striking left-lateral shear zone, which connects the Taurus collision zone in the north with the Red Sea rudimentary oceanic ridge in the south. It separates the Palestine - Sinai plate from the Arabian plate (McKenzie et al., 1970; Garfunkel, 1981).

3. DATA AND METHODOLOGY

3.1 Data

The qualitative interpretation of the data gives a simple and rough description of anomalies to have an approximate view of the geological structure of the area by an overview of size, sharpness, gradient, and position of the anomaly source bodies. Bouguer map of a scale 1: 100000 was compiled by the Egyptian General Petroleum Corporation (EGPC) as a part of the project of establishing a gravity map for Egypt with a control interval of 1 milliGal (=0.00001m/s^2). The total intensity aeromagnetic map of a scale 1:500,000 was measured with a proton magnetometer model G 816 as a field instrument with accuracy 1 nT, diurnal variation of the magnetic field was measured at base station with time interval 1 minute with instrument ENV1 MAG magnetometer with 0.1 nT accuracy after (Ismail et al., 2001).

3.2 Qualitative interpretation of Potential Data

3.2.1 Bouguer Map interpretation

The Bouguer map contains a group of positive and negative anomalies with different trends, amplitudes, sizes and shapes (Fig. 4). Regarding positive anomalies, there are six of them A, B, C, D, E and F with trends of north-northeast to east-northeast except for **F** that has a northwest-trending direction. The amplitudes of the positive anomalies range from 14 to 2 mGal (these limits belong to A and E anomalies, respectively). The anomalies **A** and **B** have the biggest width within positive anomalies. The first one shows an elongated shape, while the second anomaly has a semicircular shape. Concerning

negative Bouguer anomalies, they are denoted by **G**, **H**, **I** and **J1-J2** letters on the Bouguer map. The anomaly **G** is trended in an east-northeast direction, while **H** and **J2** are of northeast trend and finally **I** and **J1**are of the northwest trend.

The anomaly **I** has the lowest amplitude -34 mGal. According to the extension, they are ranked as the following in descending mode; **I** followed by **J1**, **J2**, **G**, and **H** respectively. All the negative anomalies are of elongated shape.

3.2.2 RTP Map interpretation:

For the aeromagnetic map, the total intensity map (Fig. 5) is reduced to pole (Fig. 6) using Geosoft Oasis Montaj (2007). Regarding the reduced to pole (RTP) map, there are six positive anomalies **A**, **B**, **C**, **D**, **E** and **F** (Fig. 6). The magnetic anomalies have different trending directions; **A**, and **F** anomalies have a north-south trend, **B** and **C** have north-northeast trend, **D** has a west-northwest trend and **E** with east-northeast trend. The amplitudes of the anomalies varied largely; the highest amplitude belongs to **B** anomaly while the lowest amplitude of the positive anomalies belongs to **F** anomaly.

The extensions of positive anomalies ordered in descending order as the following **B**, **E**, **A**, **C**, **D**, and **F**. All the positive anomalies have elongated shapes;

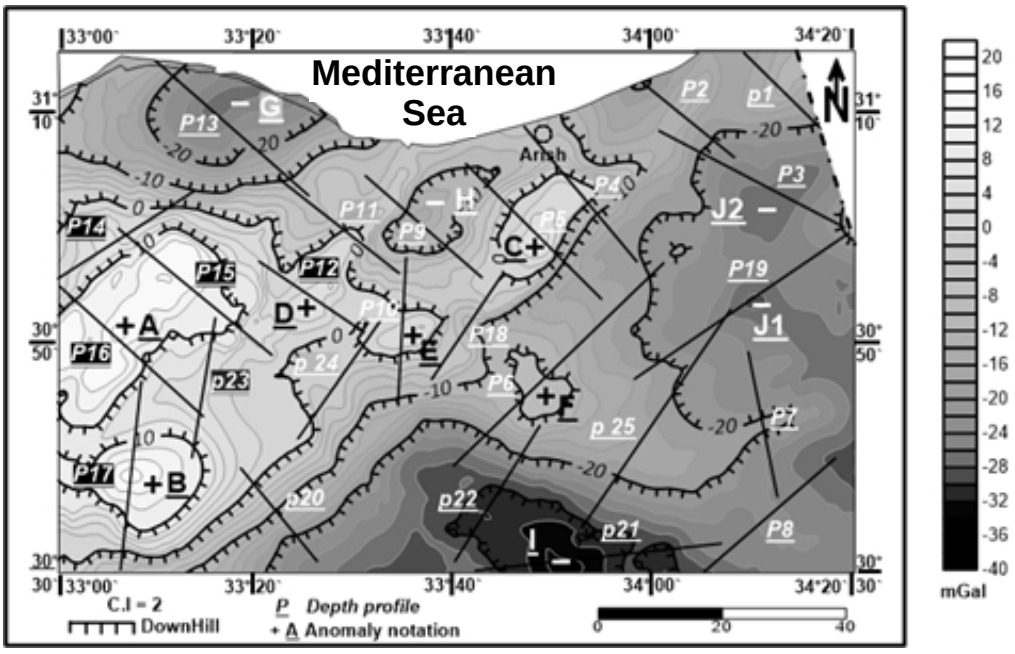

Figure 4. Bouguer map showing the locations of both major anomalies and depth profiles.

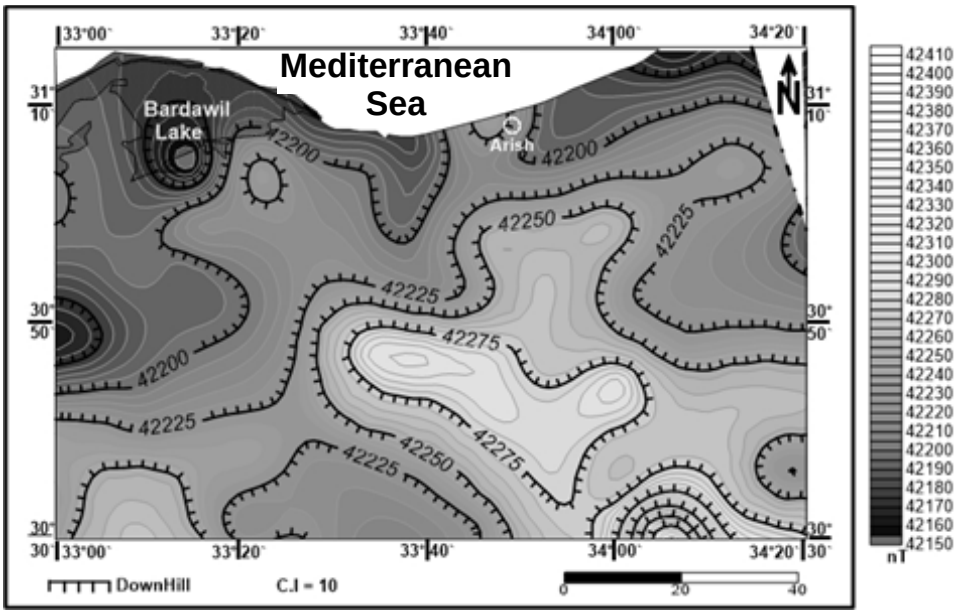

Figure 5. Total Intensity map of the study area.

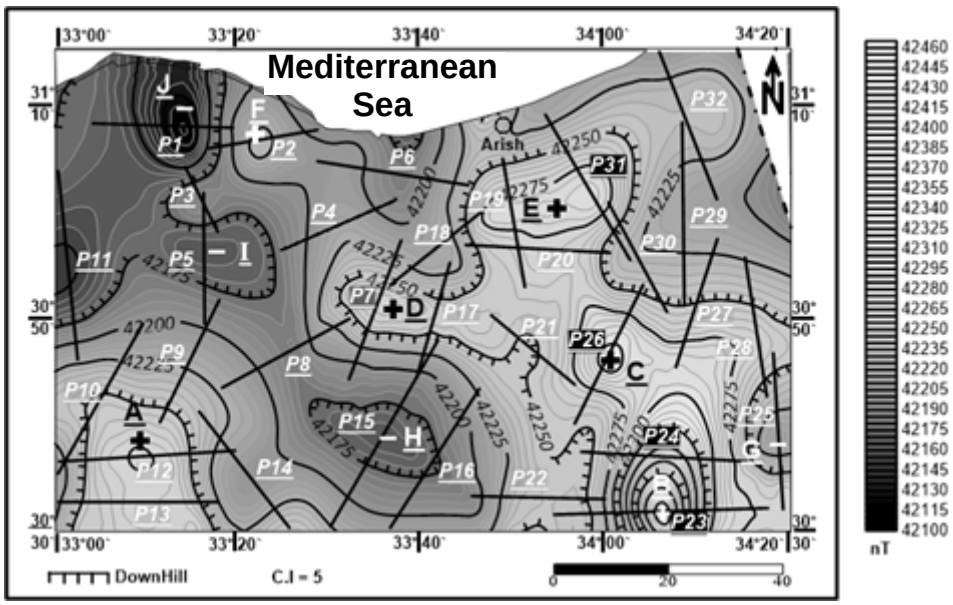

Figure 6. RTP map showing the locations of both major anomalies and depth profiles.

however, **C** anomaly could be considered semicircular. On the other hand, negative anomalies are represented by **G**, **H**, **I** and **J** that have a high concentration in the west portion of the map with trending directions; **G** with east-northeast trend, **H** and **I** anomalies with west-northwest trend and finally **J** anomaly with almost north-south tend. The anomaly **J** comes at first as the highest amplitude with 42115 nT troughs followed by **H**, **I** and **J** respectively. According to the volume, anomaly **H** is the biggest then **J** and **I** anomalies and finally **G**. All negative anomalies have an elongated shape.

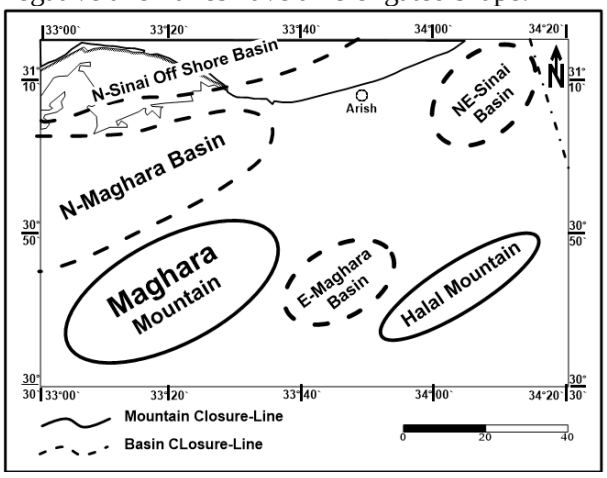

Figure 7. Location map of basins and mountains (after Abdin & Aal 1992; Sharhan & Salah 1996).

Qualitatively, there is an obvious relationship between both Bouguer and RTP maps with the geomorphological features of the area. For example, Maghara Mountain is related to anomalies "A" and "B" in Bouguer and anomaly "B" in RTP maps as obvious in (Fig. 7). Also, Halal Mountain is related to anomaly "F" in Bouguer and anomalies "C" and "B" in RTP maps.

Finally, it is obvious that there are alternated high and low structures trending in the northeast-southwest direction that indicates major tectonic events happened in the study area.

3.3 Quantitative interpretation

3.3.1 Trend analysis:

The trend analysis is a technique that helps to detect the tectonic trends that affected the area (Affleck, 1963). Defining the trends of the area gives an overview image that helps analyze the tectonic forces that affected this area.

Fault planes and the boundaries of blocks are usually having the maximum horizontal gradient (Vxz), which is the rate of change of gravity (Δg) or magnetic (Δt) fields with the distance.

The V_{XZ} values can be calculated, using Nettleton's (1940) equations:

$$\mathbf{Vxz} = \frac{g_1 - g_2}{\Delta x} \quad \text{..... (1)}$$

Or

$$\mathbf{Vxz} = \frac{t_1 - t_2}{\Delta x} \quad \text{..... (1)}$$

Where:

$\boldsymbol{g_1 - g_2}$**:** *are the observed gravity values at two successive stations 1 and 2*

$\boldsymbol{t_1 - t_2}$: *are the observed magnetic values at two successive stations 1 and 2*

(Δx): is the constant interval distance

For Bouguer, trend analysis gives seven trends the Syrian Arc trend 24.8% (N45°-65°E), Tibesti 17.8% (N25°-45° E), Tethyan 14.6% (N 85° E to N

85° W), Aqaba 9.7% (N15°-25°E), East Africa 7.9% (N 10° E-N10° W), Suez Gulf 7.9% (N25°-45°W), Najd 7.8% (N65°W) respectively arranged in decreasing order (Fig. 8). While RTP trends are different according to the measured parameters for the two geophysical methods, It is appeared that East Africa 20.4% (N 10° E-N10° W), Tethyan 18.8% (N 85° E to N 85° W), Najd 11.6% (N65°W), Aqaba 11.5% (N15°-25°E), Tibesti 7.6% (N25°-45° E), Suez Gulf 4.4% (N25°-45°W) and Syrian Arc 1.4% (N45°-65°E), respectively in a decreasing order (Fig. 9).

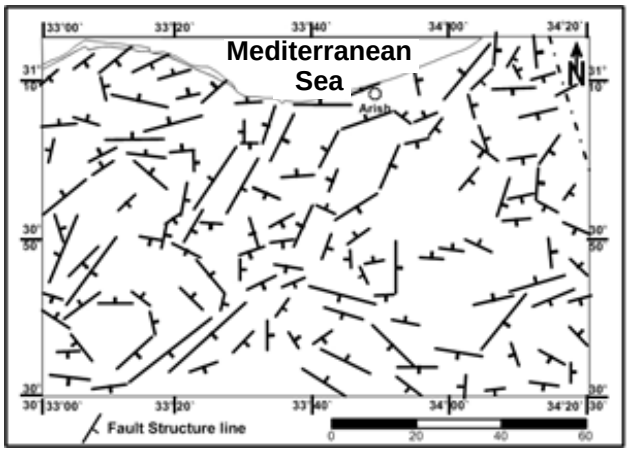

Figur. 8. Base Map for trend analysis of Bouguer map.

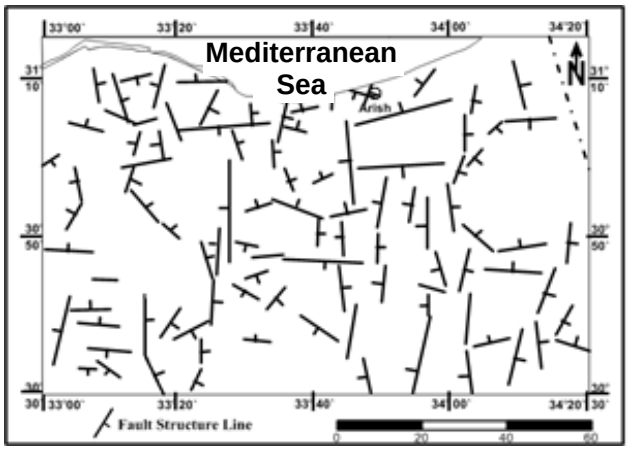

Figure 9. Base Map for trend analysis of the RTP map.

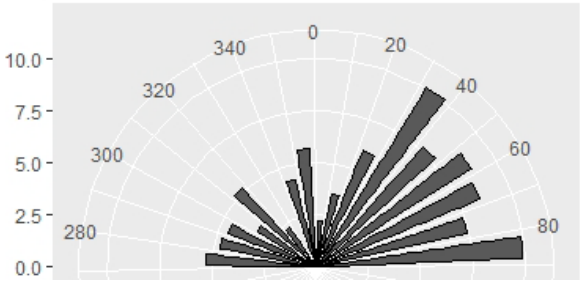

Figure 10a. Rose diagram for fault trends of Bouguer map.

A graphical representation of the calculated first horizontal gradient technique on Bouguer and RTP maps is shown and can compare in rose diagrams (Fig. 10a, b).

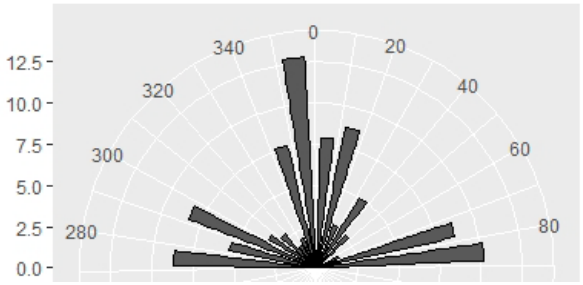

Figure 10b. Rose diagram for fault trends of RTP map

The geophysical magnetic method are concerned with measuring the magnetic field of the earth so that in addition to shallow intrusions it is mainly a measure of the relative horizontal changes within the basement rocks that extends from the basement top to the isothermal curie depth (Hinze *et al.*, 2013), while the gravity method influenced by the density of all rocks because all rocks have densities and as a result, we may have a difference between the results of the two methods.

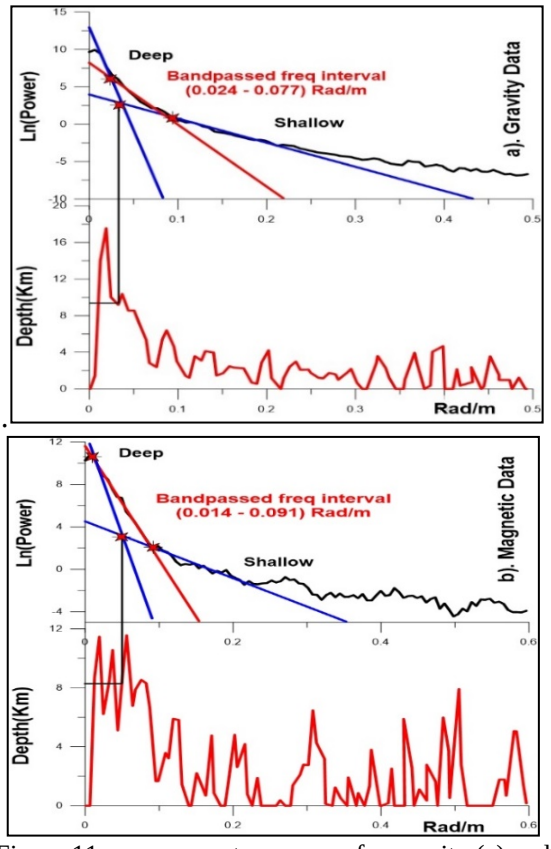

Figure 11. power spectrum curve for gravity (a) and magnetic (b) data.

3.3.2 Regional - Residual separation using the Fast Fourier Transform (FFT):

Fast Fourier Transform (FFT) filter is used to

separate different components of the data according to the frequencies by drawing the power spectrum curves for these data and separate these residual (shallow) and regional (deep) components. In our case of application- depending on its frequencies where every segment of the frequency curve is fitted to the same tangent sloped straight line related to a definite component. Moreover, the depths to source bodies of these frequencies of the potential fields can be calculated. (Sadek et al., 1984) also used this filter for getting a band passed maps for gravity and magnetic fields by passing the frequencies within the optimum interval that represents the best signal to noise ratio band of the field. Many authors discussed the spectral analysis technique such as Lee (1960) and Bhattacharyya (1966).

The Power spectrum curve of gravity data shows that there are three components related to deep, intermediate and shallow frequencies, respectively. The band-pass filtered map includes the intermediate components higher than the low regional ones (usually basement) and smaller than high ones (usually intrusions and noises). Therefore, this map can be related to the sedimentary cover of wavenumbers between 0.024 and 0.077 rad/m (Fig. 11.a). The anomalies have a major NE trend with one anomaly of NW trend directions that crossed through the NE anomalies at the center of the study area (Fig. 12). While for RTP band-pass map of the magnetic field is between wavenumbers 0.014 and 0.091 rad/m (Fig.11b). The anomalies have a major NW trend crossed by an N-S trend (Fig. 13).

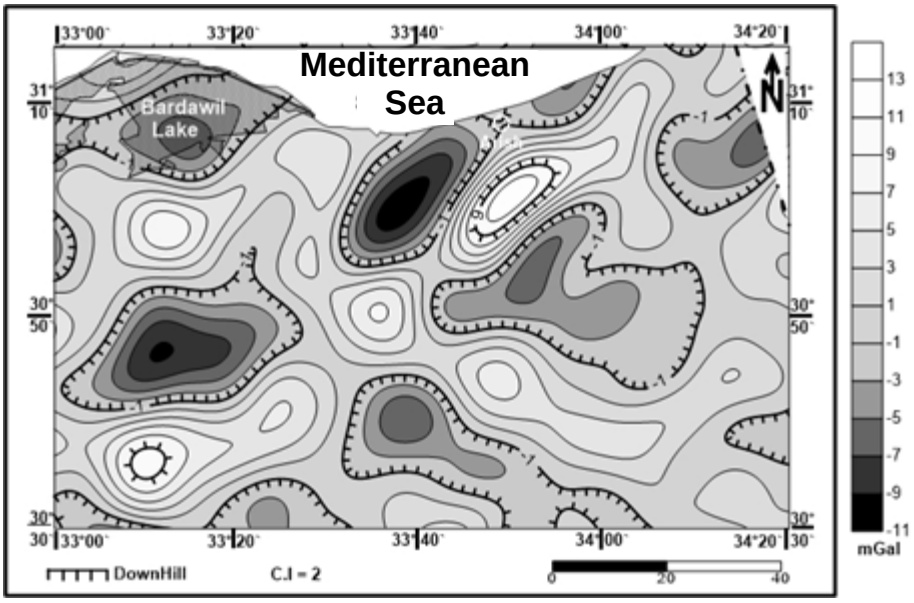

Figure 12. Bandpass Gravity map between wavenumbers 0.024 and 0.077 rad/m.

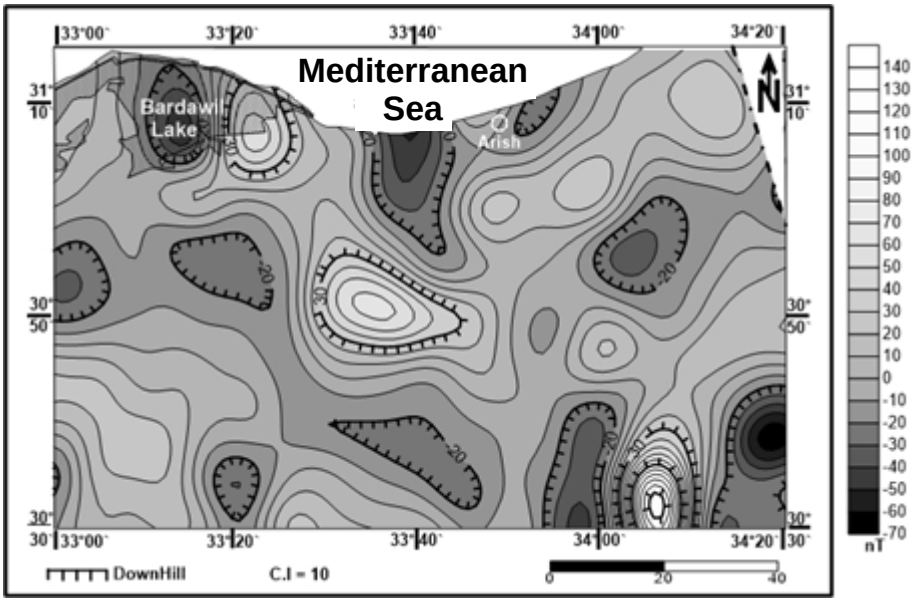

Figure 13. Bandpass RTP map between wavenumbers 0.014 and 0.091 rad/m.

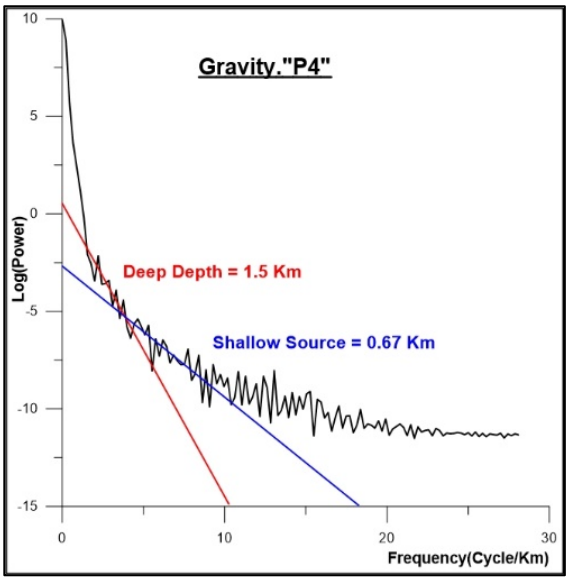

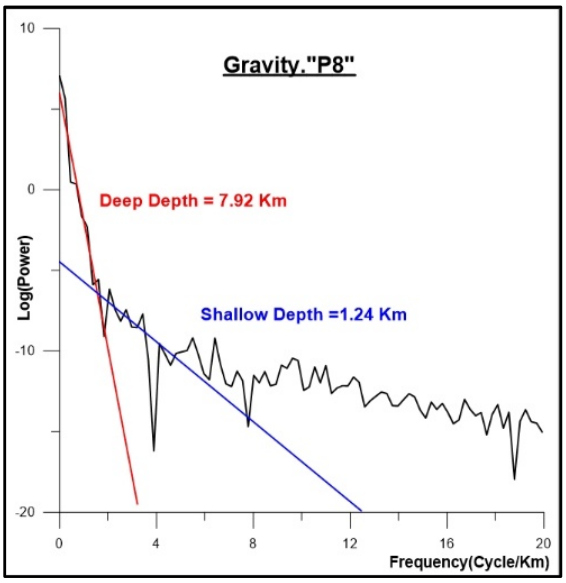

Figure 14. Depth Estimation of gravity profiles no. 4 & 8 using spectral analysis.

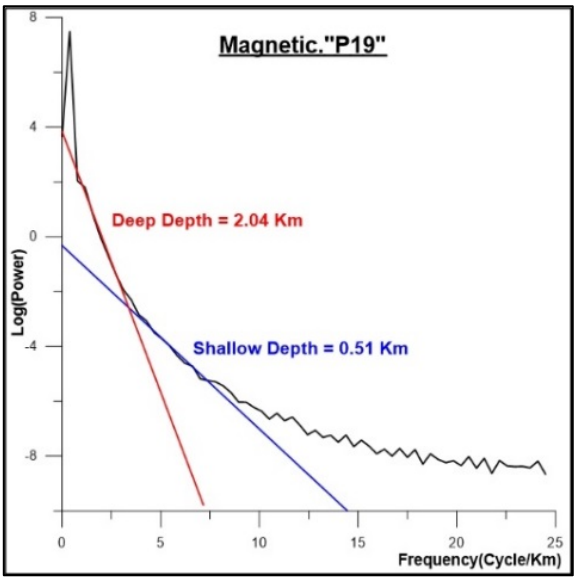

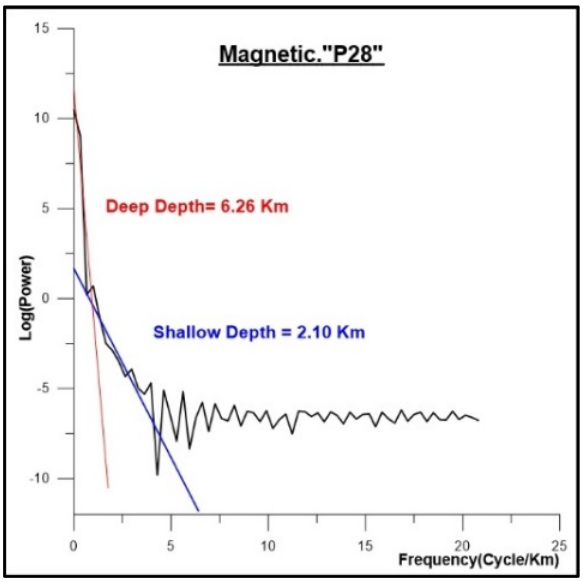

Figure 15. Depth Estimation of magnetic profiles no. 19 & 28 using spectral analysis.

3.3.3 Depth estimation

The depth estimation is carried out to calculate the depth to the causative bodies of different anomalies, in addition, to give an idea about the thickness of the sedimentary cover, which will be useful for locating the basins and also the depth to intrusions in the area. We used (Spector & Grant, 1970) method is used to determine the depth of gravity and magnetic sources by converting the selected gravity and magnetic profiles from the space domain to the frequency domain. The depth values extracted from the depth profiles are shown in Table (1) range from 1.5 to 7.9 km for gravity data, and from 2 to 6.3 km for magnetic profiles figures (14 and 15).

3.3.4 Basement Structure Map

The Bouguer residual maps were manipulated

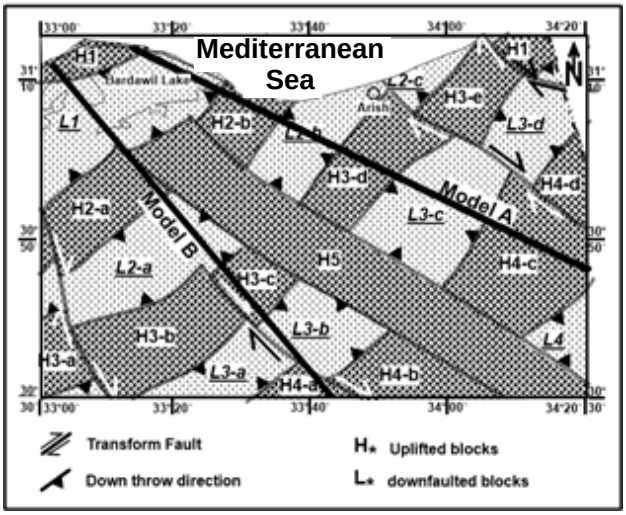

Figure 16. Structure Map of the Area.

for configuring the tentative structural map, where the positive anomalies interpreted as uplifted basement blocks and the negative anomalies interpreted as down-faulted blocks. The map gives two sets of faults affecting the area. The first set consists of normal faults of NE-SW trending direction resulting in a set of alternating Horst/Grabben structure intersected by four transform faults from the northeast corner to southeast one aligned in NW-SE direction perpendicular to the NE-SW uplifted/down faulted blocks. Generally, there are several uplifted/horst blocks marked from H1 – H5, in addition to down-faulted blocks numbered from L1-L4 as illustrated in (Fig. 16).

3.3.5 The gravity and magnetic modeling

The measured gravity field is controlled by the spatial density and elevation variation of the subsurface geological structure from the regional scale. Although the gravity data cannot be the mirror of the density distribution within the earth's interior Solely (Tealeb & Riad, 1986), Bouguer anomalies are highly related to the crustal thickness (Woolard, 1959; Pick et al., 1973; Riad et al., 1983; Riad & EI-Etr, 1985).

Table 1. Depth profiles values in kilometers for both gravity and magnetic data.

Gravity Depth Estimation			Magnetic Depth Estimation					
Profile	Deep	Shallow	Profile	Deep	Shallow	Profile	Deep	Shallow
p1	1.32	0.44	p1	2.13	0.61	P26	5.74	0.82
p2	2.48	0.61	p2	3.04	0.98	P27	3.01	0.67
p3	3.07	0.87	p3	2.59	------	P28	6.26	2.10
p4	1.5	0.67	p4	2.93	0.66	P29	4.76	0.8
p5	4.97	1.11	p5	2.98	0.74	P30	2.99	0.88
p6	3.88	0.95	p6	2.89	0.64	P31	3.7	0.95
p7	2.72	0.63	p7	2.48	0.96	P32	3.08	0.47
p8	7.92	1.24	p8	3.5	0.68	---------	---------	---------
p9	1.16	0.44	p9	2.6	0.66	---------	---------	---------
p10	1.56	0.43	p10	4.38	1.4	---------	---------	---------
p11	4.44	0.93	p11	2.45	0.47	---------	---------	---------
p12	2.97	0.57	p12	4.91	------	---------	---------	---------
p13	3.79	1.33	p13	5.87	0.97	---------	---------	---------
p14	3.61	1.45	p14	3.96	1.01	---------	---------	---------
p15	4.19	0.81	p15	6.22	1.39	---------	---------	---------
p16	3.96	0.72	p16	5.78	0.53	---------	---------	---------
p17	5.38	1.39	p17	2.91	0.71	---------	---------	---------
p18	2.22	0.82	p18	1.38	0.65	---------	---------	---------
p19	4.12	0.68	p19	2.04	0.51	---------	---------	---------
p20	1.42	0.43	p20	2.97	0.86	---------	---------	---------
p21	5.97	0.7	p21	3.08	0.47	---------	---------	---------
p22	2.37	0.6	p22	2.39	0.66	---------	---------	---------
p23	2.97	0.8	p23	4.08	0.75	---------	---------	---------
p24	3.76	0.7	p24	3.53	1.06	---------	---------	---------
p25	2.05	0.71	p25	5.47	1.2	---------	---------	---------

Table 2. Schedule for densities of the sediments, Upper, Lower Crust and Mantle in different studies

Previous Studies	Sediments	U. Crust	L. Crust	U. Mantle
Jacobs et al. (1959)	-----	**2.67**	**3.00**	**3.30**
Makris (1976)	-----	**2.82**	**2.90**	**3.34**
Ginzburg & Ben Avraham (1987)	**2.50**	**2.80**	**2.96**	**3.25**
Abdelrahman et al. (1988)	**2.45**	**2.68**	**2.90**	
Setto, 1991	**2.46**	**2.68**	**2.90**	**3.30**
Omran & Fathy, (1998)	**2.30**	**2.67**	**3.00**	**3.30**
Ismail (1998)	**2.40**	**2.70**	**3.10**	**3.47**
Omran (2001)	**2.37**	**2.67**	**3.07**	**3.44**
Salem et al. (2004)	**2.41**	**2.75**	**2.9**	**3.3**
El-Khadragy et al. (2010)	**2.43**	**2.74**	**2.93**	**3.28**
Saada et al (2014)	**U 2.10 - L 2.50**	**2.7**	**2.93**	**3.33**
This Study	**U 2.4 - M 2.6 - L 2.5**	**2.67**	**-----**	**-----**

On the other hand magnetic field is connected to the magnetic susceptibility of the underlying rocks and also limited to the isothermal Curie depth at which the rocks can't be polarized, which means that the magnetic field is shaped by the susceptible rocks that are almost found between the top of basement rocks and the isothermal curie depth. (Morgan et al., 1977) stated that the isothermal Curie depth is about 16.8-18 km by a studying the geothermal gradient in north Egypt and Gulf of Suez using the drilled wells, and (Aboud et al., 2011) stated an averaged Curie depth nearby the study area to be 16-18 km by a study of the geothermal gradient of Sinai Peninsula. The depth to the bottom of the source is recorded where a maximum peak is represented (Hinze et al., 2013). According to (Sadek et al., 1984), the maximum slope of the fitted tangent is divided by (4π) for calculating the isothermal curie depth of the study area 15.5 km. The densities of the rocks in the study area were defined by the correlation and comparison of rock densities used in numerous studies (Table 2) that were carried out in different regions of Egypt and also the most compatible values for the present models.

3.3.6 The results of 2-D gravity and magnetic modeling

In this study, sediments are divided into upper (Cenozoic), middle (Mesozoic) and lower (Paleozoic) layers with densities of 2.4, 2.6, 2.5 g/cm^3 respectively. It is obvious that the Mesozoic part has the highest density and that because the Mesozoic lithostratigraphic section consists of almost limestone/dolomite facies that have high densities. The models comprise also the uppermost part of the crust that is limited between the isothermal Curie depth and the top of the basement. The crust is subdivided into adjacent faulted blocks with densities and susceptibilities that differ from one block to another (Hinze et al., 2013). The geometry and the extension of the modeled blocks are configured by the constructed structure blocks in addition to the estimated depth of the Curie point. Sukot-1 well is used as a starting point in the models; it has a total depth of 3.41 km that reaches middle Jurassic time.

The first profile (Mod A) trends WNW- ESE (Fig. 16), with gravity and magnetic anomalies values ranges from -9.12 to 11.63 mGal and from -42 to 43nT respectively. This profile comprises the uppermost crustal faulted blocks (Fig. 17), with density values ranging from 2.66 g/cm^3 for H1 to 2.69 g/cm^3 for H3. On the other hand, magnetic susceptibility in the CGS-units ranges from .00011 for H1 to .0032 for L1. The basement depth averaged about 7Km with a maximum and minimum values recorded at L2 and H2 respectively.

While the second profile (Mod B) trends NNW-SSE (Fig. 17), with gravity and magnetic anomalies values fluctuated between -9.12, 11.63 mGal and -42, 43nT respectively (Fig. 18). The basement faulted blocks have densities between 2.66 g/cm^3 for L2 and H4 and 2.71 g/cm^3 for H1. In the concern of the magnetic field, magnetic susceptibility in the CGS-units for the block ranges from .0001 for L3 to .0011 for H1. The averaged basement depth is about 8Km with a maximum and minimum values recorded at L2 and H1 respectively. Both models show that the area influenced by normal faults with different angles and throw values that affected both the basement and the sedimentary sections.

The density and susceptibility value related to the constructed models indicate an acidic composition of the deep-seated basement rocks. The study area covered by a thick sedimentary cover that reaches 7.5 km thickness, in addition to the geologic structures of the area, along with the oil and gas explorations in the neighborhood makes it a highly promising area for upcoming oil and gas investigations.

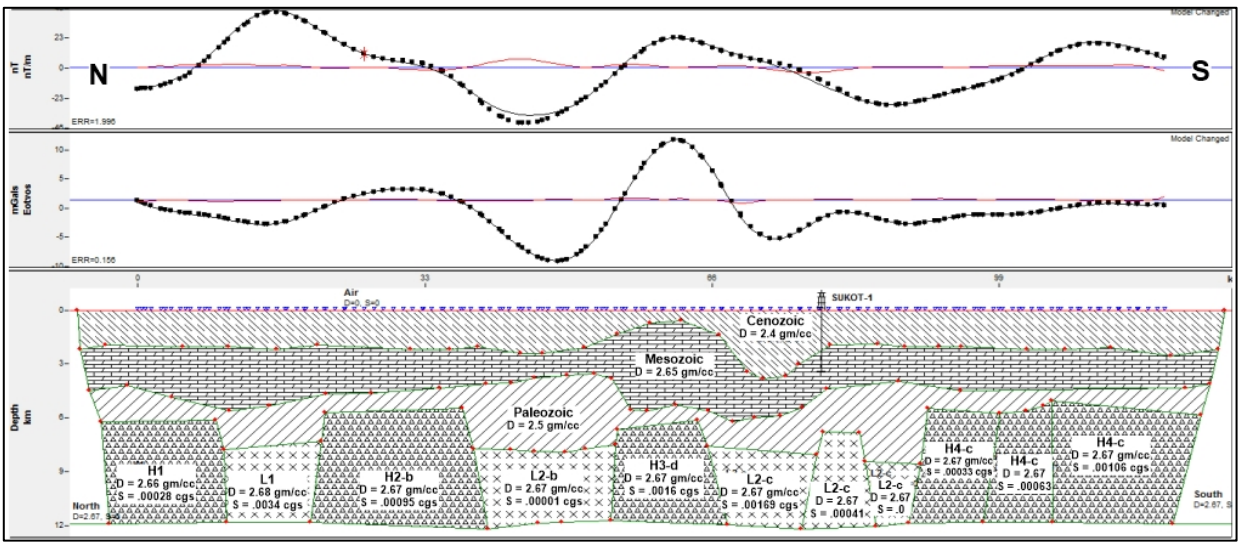

Figure 17. Geological Structure model A.

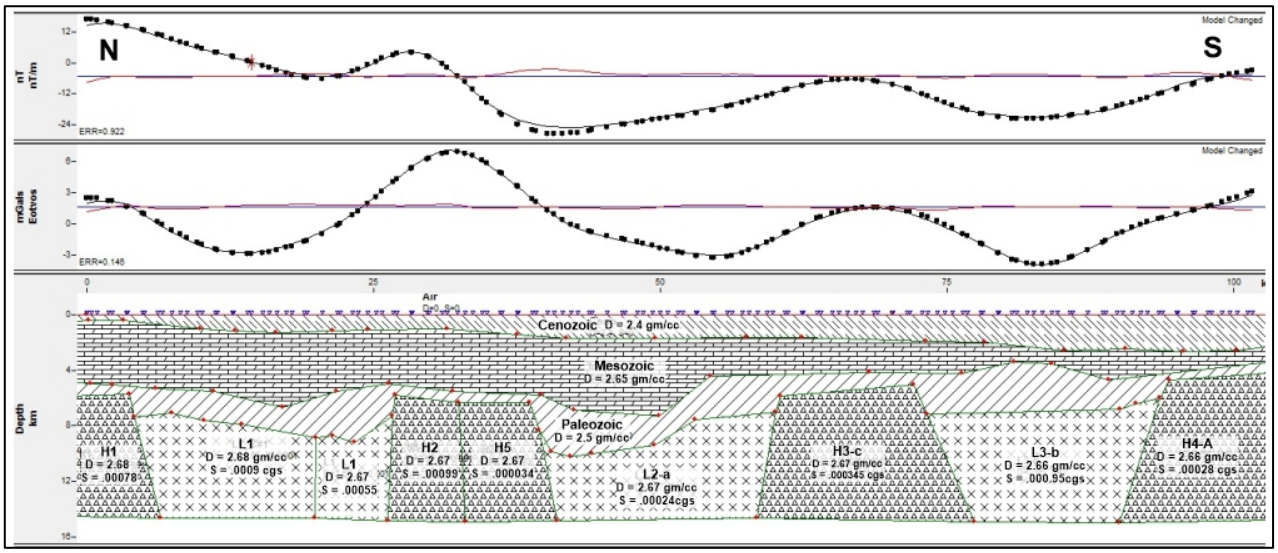

Figure 18. Geological Structure model B.

4. CONCLUSIONS

By using different analytical techniques for gravity and magnetic data that leads to deduce that:

i. The area is affected by the following trends; *Syrian Arc trend (N45°-65°E), Tibesti (N25°-45° E), Tethyan (N 85° E to N 85° W) trends* for gravity and *E-Africa (N 10° E-N10° W), Tethyan (N 85° E to N 85° W), Najd 11.6% (N65°W)* for magnetic, respectively.

ii. The regional - residual separating technique was applied on the Bouguer and RTP maps for separating the fields of shallow causative bodies from the deep one using the FFT technique. Bandpass maps are constructed for both Bouguer and RTP maps with frequency bands (low .024 – high .077 rad/Km) for gravity bandpass map, and (low .014 – high .091 rad/Km) for magnetic bandpass map. Both of these maps comprise alternating positive and negative anomalies covering the area. The average depth to the anomalies causative bodies is calculated from the power spectrum curve by spectral analysis technique after (Sadek *et al*, 1984) to be for 3.4 km and 3.6 km for gravity and magnetic data respectively.

iii. Structure map is constructed depending on the results of regional - residual separation methods mainly of gravity with magnetic data. It shows that the area consists of alternated uplifted and down-lifted blocks trending in the northeast direction. These faulted blocks are intersected by younger NW to NNW strike-slip faults (could be related to the Gulf of Suez structure).

iv. The depth to the causative bodies was calculated along 57 gravity and magnetic profiles, using the spectral analysis technique. The depths vary between 2 and 8 km.

v. Two coupled gravity and magnetic structural models are constructed to show the subsurface the structure and the geometry of the sedimentary sections (Cenozoic - Mesozoic - Paleozoic) and the uppermost part of the basement with the averaged density of 2.4, 2.6, 2.5, 2.67 g/cm^3 respectively. The magnetic susceptibility of the basement rock in CGS-units ranges between 0.00011 and 0.0032. The density and susceptibility values in the models indicate an acidic basement type. The area has a thick sedimentary cover that reaches 7.5 km. the area is rich in geologic structure in addition to the thick sedimentary cover along with the oil and gas explorations in the neighborhood areas; all these facts make it a promising area for hydrocarbon accumulations.

REFERENCES

Abdelrahman, E.M., Refai, E.M. & El-Ghalban, H.M., 1988. *Gravity models of the Nile Delta basin Egypt.* EGS Proc of 6th Ann Meet, 27-42.

Abdin, S. & Aal, A., 1992. *Impact of oil exploration on Sinai development*.3rd Conference on Sinai Development Ismailia. 1, 281-288.

Aboud, E., Salem, A. & Mekkawi, M., 2011. *Curie depth map for Sinai Peninsula, Egypt deduced from the analysis of magnetic data.* Tectonophysics 506 (2011), 46–54

Affleck, L., 1963. *Magnetic anomaly trend and spacing patterns.* Geophys 28: 379 - 395.

Al Far, D.M., 1966. *Geology and Coal Deposits of Gebel Maghara, Sinai.* General Egyptian Organization for Geological Research and Mining Geol. Survey Paper, 37, 59

Ammar, G. & Afifi, T. (1992). *Early-Late Cretaceous reef complex facies in north Sinai, Egypt (a model for oil exploration)*. 11th EGPC Exploration Seminar, Egypt, 1,577- 587.

Barakat M.G., 1982. *General review of petroliferous provinces of Egypt with special emphasis on their geologic setting and oil potentialities Petro*. Gas Proj.Cairo University, MIT, 86

Bein, A. & Gvirtzman, G., 1977. *A Mesozoic fossil edge of the Arabian plate along the Levant coastline and its bearing on the evolution of th eastern Mediterranean*. In: Biju-Duval, B. and MONATDERT, I.(eds) Structural History of the Mediterranean Basins. Paris, 95-110.

Beyth M., 1981. *Paleozoic vertical movements in Umm Bogma area, southwestern Sinai*. AAPG Bulletin, 65, 160-165.

Bhattacharyya, B.K., 1966. *Continuous spectrum of the total-magnetic field anomaly due to a rectangular prismatic body*. Geophysics 31: 97–121.

Biju-Duval B., Dercourt J. & Le Pichon X., 1977. *"From the Tethys Ocean to the Mediterranean Seas: a plate tectonic model of the Western Alpine system"*. Structural history of the Mediterranean basins, Split Symp., Ed. Technip, 143 - 164.

Biju-Duval., B. & Dercourt, J., 1980. *Les bassins de Ia Mediterranean orientale represententils les restes d'un domaine oceaniques, Ia Mesogee, ouvert au Mesozoique et distinct de Ia Téthys.* Bull. Soc. Geol. France 1980(7), 43.60.

Chenet, I.Y., & Letouzey, J., 1983. *Tectonique de Ia zone comprise entre Abu Durba et Gebel Mezzazat (Sinai Egypte) dans le contexte de evolution du rift de Suez.* Bulletin Centres Recherche Exploration - Production.Elf-Aquitaine, 7, 201—215.

EGPC, 1986. *Activity of oil exploration in Egypt (1886-1986)*. 8th EGPC Exploration Seminar, Egypt, 175.

EGPC, 1994. *Nile Delta and North Sinai Fields, Discoveries and Hydrocarbon Potential*. The Egyptian General Petroleum Corporation, 387.

EGS, 1981. *Egyptian Geologic Survey, Geologic Map of Egypt*.

El Khadragy, A. A., Saad, M. H. & Azab, A., 2010. *Crustal Modeling of South Sitra Area, North Western Desert, Egypt Using Bouguer Gravity Data*. Journal of Applied Sciences Research. 6: (1), 22-37.

El Shazly, E. M., Abdel Hady, M. A., El Ghawaby, M. A. & El Kassas, I. A., 1974. *Geology of Sinai Peninsula from the ERTS-1 satellite images, Remote Sensing Research Project* Acad. Sci. Res. Technol., Cairo.

Freund, R., Garfunkel, Z., Zak, I., Goldberg, M., Weissbrod, T. & Derin, B., 1970. *The shear along the Dead Sea Rift.* Philos. Trans. R. Soc. London, 267A, 107-130.

Garfunkel, Z., 1981. *Internal structure of the Dead Sea leaky transform (rift) in relation to plate kinematics*. Tectonophysics 80, 81—108

Ginzburg, A. & Ben Avraham, Z., 1987. T*he deep structure of the central and southern Levant continental margin*. Annual.Tectonicae. 1, 105-115.

Hinze, W.J., Von Frese, R.R.B. & Saad, A.H., 2013. *Gravity and Magnetic Exploration Principles, Practices, and Applications.* Cambridge Univ Press.

Hsu, K. J., 1977. *Tectonic evolution of the Mediterranean basins.* In: A.E.M. Naim, WH. Kanes and EG. Stehli (eds), The ocean basins and margins 4(A): 29-75, Plenum Press, New York.

Ismail, M. A., 1998. *Geophysical studies in northern part of Egypt.* Ph.D. Thesis, Cairo University.

Ismail, A.M., Sultan, A.S. & Mohamady, M.M., 2001. *Bouguer And Total Magnetic Intensity Maps of Sinai Peninsula, Scale 1:500,000.* Proc 2nd International Symposium on Geophysics, Tanta, 111-117.

Jacobs, J. A., Russall. R. D. & Tuzo, W. J., 1959. *Physics and Geology*. McGraw-Hill, Tronto.

Jenkins, M., Harms, J.C. & Oesleby, T.W., 1982. *Mesozoic sediments of Jebel Maghara, north Sinai, Egypt.* 6th EGPC Exploration Seminar, Egypt, I, 1-23.

Le Pichon, X. & Francheteau, J., 1978. *A plate-tectonic analysis of the Red Sea-Gulf of Aden area, in Oren.* OH, ed., Structure and tectonics of the eastern Mediterranean: Tectonophysics, 46, 369—406.

Lee, Y.W., 1960. *Statistical Theory of communication.* Willey and Sons, New York, 1 - 75.

Makris, J., 1976. *A dynamic model of the Hellenic Arc deduced from geophysical data*. Tectonophysics. 36, 339-346.

Mckenzie D.P., Davies D. & Molnar P., 1970. Plate tectonics of the Red Sea and East Africa Nature, 226 (1970), 243-248.

Monod, O., Marcoux, J., Poisson, A. & Dumont, J.F., 1974. *Le domaine d'Antalya, témoin de la fracturation de la plateforme africaine au cours du Trias. Soc. Géol. France Bull.*, 16, 116–127.

Morgan P (1990). *Egypt in the framework of global tectonics. In: Said (ed) The Geology of Egypt*, Balkema, Rotterdam, 91–111.

Morgan, P., Blackwell, D.P., Farris J.C., Boulos, F.K. & Salib P.G., 1977. *Preliminary geothermal gradient and heat flow values for north Egypt and Gulf of Suez from oil well data*. Proc Intl Congr Thermal Waters, Geothermal Energy and Volcanism of the Mediterranean area (1976), Nat Tech Athens, 424-438.

Neev, D., 1975. *Tectonic evolution of the Middle East and Lavantine basin (easternmost Mediterranean)*. Geology, 3, 683-686.

Neev, D., 1977. *The Pelusium Line: A major transcontinental shear*, Tectonophysics, 38, Tl-T8.

Neev, D., Hall J.K. & Saul J.M., 1982. *The Pelusium megashear system across Africa and associated lineament swarms.* J. Geophys. Res., 87(B2), 1015-1030.

Omran, M.A. & Fathy, H., 1998. *Structural evolution of the Nile cone area.* Egypt. Journal. Geology. 42: (1), 273-291.

Omran, M.A., 2001. *Crustal modeling of central Nile Delta region*. Annual. Geol. Survey.

Pick, M., Picha J. & Vyskocil, V., 1973. *Theory of Earth`s gravity field.* Academia, Publ Hause of Czechoslovak academy of sciences.

Rabeh, T. & Khalil A., 2015. *Characterization of fault structures in southern Sinai Peninsula and Gulf of Suez region using geophysical data.* Environmental earth sciences, Springer Berlin Heidelberg 5, 1925-1937

Riad, S. & El-Etr, H.A., 1985. *Bouguer anomalies and lithosphere- crustal thickness in Uganda*. Journal of Geodynamics 3, 169-186.

Riad, S., Fouad A., Refai E. & Ghaleb M., 1983. *Preliminary interpretation of regional gravity anomalies of Egypt.* Paper presented at the 8th General Assembly of the IUGG, Hamburg.

Robson, D.A., 1971. *The structure of the Gulf of Suez (Clysmic) rift with special reference to the eastern side*. J. Geol. Soc., London, 127, 247-177.

Saada, S.A., Zahra, H. & El-Khadragy, A.A., 2014. *Structural Pattern and Crustal Modeling of the Central Northern Part of Egypt, Using Bouguer Gravity Data*. Journal of Applied Sciences Research. 9: (10), 6373-6386.

Sadek, H.S., Rashad, S.M. & Blank, H.R., 1984. *Spectral analysis of aeromagnetic profiles for depth estimation principles, software, and practical application*. USGS Publications Warehouse SN - 84-849.

Said, R., 1962. *The geology of Egypt*. Elsevier Publishing Co, Amsterdam.

Said, R., 1990. *Cenozoic. In: Said R (ed) The geology of Egypt.* Balkema, Rotterdam, 451–486.

Salem, S. R., El-Khateeb, S. O. & Mousa. M. F., 2004. *Structure and evolution of North African passive margin crust: As inferred from 2-D gravity modelling of Nile Delta and its surrounding areas, Egypt.* Egyptian Geophysical Society Journal. 2: (1), 17-29.

Selim, E.S.I., 2015. *The integration of gravity, magnetic and seismic data in delineating the sedimentary basins of northern Sinai and deducing their structural controls.* Journal of Asian Earth Sciences.

Setto, I. A., 1991. *A crustal model for the Nile Delta, Egypt*. Journal. Geol. 34: (1-2), 279-292.

Sharhan, A.S. & Salah, M.G., 1996. *Geologic setting and hydrocarbon potential of north Sinai, Egypt.* Bulletin of Canadian Petroleum Geology, 44, 4, 615-631.

Shata, A., 1956. *Structural development of the Sinai Peninsula, Egypt*. Desert Institute of Egypt, Bulletin, 6, 22.

Smith, J.G., 1971. *Alpine deformation and the oceanic areas of the Tethys, Mediterranean and Atlantic*. Geol. Soc. Amer. Bull., 82, 2039.

Smith, **M.,** 1984. *Well evaluation Conference*. In "Schlumberger", Egypt.

Spector, A. & Grant, F.S., 1970. *Statistical models for interpreting aeromagnetic data*. Geophysics, 35, 293-302

Steckler, M., 1985. *Uplift and extension at the Gulf of Suez-indication of induced mantle convection*. Nature, 317, 135-139.

Tealeb, A. & Riad S., 1986. *Regional gravity anomalies of western Saudi Arabia and their geological significance*. EGS Proc of 5th Ann Meet March 29-30:50- 89.

Woolard, G.P. 1959. *Crustal structure from gravity and seismic measurements*. J of Geoph Res 64,1521-1544.

Zaghloul, Z. & Khidr, I., 1992. *Subsurface Geological Setting of the Mesozoic-Cenozoic formations and hydrocarbon potentials, north Sinai*. 11th EGPC Exploration Seminar, Egypt, 1, 563-577.

Received at: 26. 10. 2019
Revised at: 21. 02. 2020
Accepted for publication at: 26. 02. 2020
Published online at: 28. 02. 2020